A New Method and Results of Estimating Areal-Mean Spectral Surface Albedo from Downwelling Irradiance Measurements

Z. Li and M. C. Cribb
The Earth System Science Interdisciplinary Center
University of Maryland
College Park, Maryland

A. P. Trishchenko
Canada Centre for Remote Sensing
Ottawa, Ontario, Canada

Introduction

Areal-mean surface spectral albedo is a fundamental surface parameter required for various modeling and remote sensing studies. Ground-based observations can only represent a very small area and surface albedo often varies greatly at small spatial scales and throughout the different seasons (Ohmura and Gilgen 1993). For modeling and remote sensing studies, areal-mean surface albedo representative of an area comparable to a model grid or a satellite pixel is needed. The vegetative land cover surrounding the Atmospheric Radiation Measurement (ARM) Central Facility (CF) site is so variable that point-wise measurements of surface albedo do not provide reliable surface albedo data. Satellite images of the area surrounding the CF for different seasons illustrates this seasonal variability in land cover (Figure 1).

We propose a novel method to estimate areal-mean surface spectral albedo from downward surface irradiance measurements made under overcast conditions. The method relies on good information on cloud parameters (liquid water path [LWP], effective radius [r_e], etc.) extracted from such instruments as the Millimeter Wavelength Cloud Radar (MMCR) and Microwave Radiometer (MWR) and spectral transmittance of solar irradiance as measured by the Rotating Shadowband Spectroradiometer (RSS). The method is tested for overcast skies containing a low-level non-precipitating cloud. It was validated

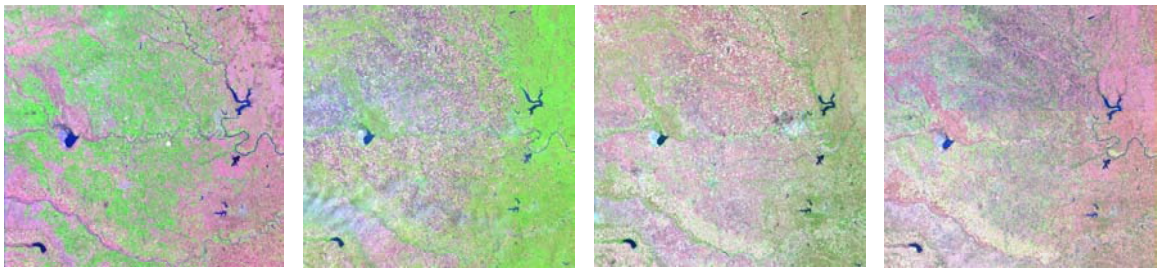

Figure 1. Landat 7 enhanced thermatic mapper plus (ETM+) images of area surrounding the CF (off-centre in images) for the four seasons in the year 2000. From left to right, images are for the following dates: April 4, June 7, September 11, and November 14. Images cover an area of roughly 20 by 20.

using some field campaign measurements and applied to numerous cloudy cases encompassing all seasons. The results were compared with point-wise surface albedo data deduced from upwelling and downwelling irradiance measured by the Multi-filter Rotating Shadowband Radiometer (MFRSR).

Data Selection and Modeling Fluxes

Overcast cloudy cases were identified utilizing information from the large array of instruments installed at the CF site. These include broadband measurements of downward surface fluxes from the Baseline Surface Radiation Network Radiometer for identifying periods when little direct flux reached the surface, indicating the presence of a cloudy obstruction; MMCR snapshots showing whether the cloud was single-layered; and for determining if it was precipitating, rain gauge measurements from the Surface Meteorological Observing Station. Ancillary information, such as the state of ground conditions at the CF, were culled from weather observations collected by on-site personnel. When available, satellite-observed radiance fields from the Visible Infrared Scanning Radiometer (VIRS) aboard the Tropical Rainfall Measuring Mission satellite at visible and infrared wavelengths were used to identify the phase (water/ice) of the cloud field in the vicinity of the CF. The final screening for selecting cases depended on the availability of high-resolution solar spectral irradiance data from the RSS (360-1050 nm, 1024 channels), an instrument developed at the Atmospheric Sciences Research Center at the State University of New York in Albany and in operation at the CF since August 1997 (Harrison et al. 1998). After analysis of ARM data at the CF from August 1998 until October 2000, 19 days, encompassing all seasons and fulfilling the requisite cloudy conditions, were examined.

The latest version of the Moderate-Resolution Atmospheric Radiance and Transmittance Model 4 (MODTRAN4) radiative transfer code (Anderson et al. 1999) was used to model fluxes. Radiosonde soundings provided atmospheric profiles of pressure and temperature. Total column amounts of water vapor and liquid water were obtained from MWR retrievals. Water vapor mixing ratio profiles were calculated from the humidity, pressure and temperature profiles and scaled to MWR retrievals. Satellite data from the Total Ozone Mapping Spectrometer provided ozone column amount. Initial values of surface albedo were obtained from the MFRSR. Cloud top boundaries were determined using reflectivities measured by the MMCR; ceilometer observations were used to set the cloud base heights. Vertical profiles of liquid water content were derived using the method of Frisch et al. (1995). Cloud optical properties were obtained from tuning the extinction coefficient, β, at 500 nm to achieve agreement between the simulated and RSS-measured downward surface fluxes in this spectral band. Effective radius was then calculated as $r_{eff} = 1.5\ LWP / (\beta\ \Delta z)$, where Δz is the cloud layer thickness. Microphysical properties of the water cloud were modeled using Mie theory. The cases are summarized in Table 1.

Estimating Areal-Mean Albedo

Estimation of areal-mean albedo is founded on the idea that a uniformly overcast sky acts as a reflector of photons between the surface and the cloud base and that photons received at some ground-based observational platform, such as the RSS, may have been reflected from vegetative surfaces quite a distance away, hence possess spectral information about those surfaces. The goal of the method is to retrieve this surface spectral information from downwelling radiation measured by the RSS.

Table 1. Description of overcast cases studied here.

Date	UTC Time	Col. Amt. (cm) WV	LW	O_3	Cloud Position (km)	τ	R_{eff} (μm)
971019	17:30	1.6	0.007	0.34	0.57 - 0.85	17.9	5.9
	17:35	1.6	0.007	0.34	0.61 - 0.85	15.8	6.8
	17:40	1.6	0.007	0.34	0.58 - 0.85	17.4	5.8
	17:45	1.6	0.007	0.34	0.59 - 0.85	15.7	6.6
	17:50	1.6	0.008	0.34	0.58 - 0.85	16.5	7.2
	17:55	1.6	0.008	0.34	0.60 - 0.86	21.1	5.7
	18:00	1.6	0.009	0.34	0.61 - 0.86	20.8	6.6
	19:00	1.6	0.015	0.34	0.55 - 0.94	36.4	6.0
971020	14:30	2.3	0.027	0.29	0.84 - 1.40	36.8	10.9
971026	21:00	1.2	0.007	0.34	0.77 - 1.02	14.4	7.6
971106	15:30	0.7	0.001	0.29	0.64 - 0.78	7.8	2.6
971210	20:30	0.9	0.008	0.34	0.76 - 1.20	22.9	5.2
971212	18:00	0.4	0.005	0.34	0.73 - 0.97	18.6	3.8
971222	17:30	1.4	0.002	0.34	0.58 - 1.00	10.0	2.9
971225	19:30	0.9	0.027	0.36	0.62 - 1.27	54.3	7.6
	19:40	0.9	0.013	0.36	0.87 - 1.27	35.2	5.7
	19:50	0.9	0.015	0.36	0.83 - 1.23	29.7	7.8
980113	20:30	1.0	0.012	0.33	0.45 - 1.00	27.7	6.6
980208	20:55	1.4	0.005	0.33	1.50 - 1.80	7.1	10.1
980330	18:30	2.8	0.008	0.34	0.34 - 0.75	12.5	10.0
980403	18:39	1.4	0.034	0.38	1.00 - 1.50	55.1	9.3
980429	20:30	1.9	0.043	0.40	0.82 - 1.42	65.0	10.0
980604	14:15	4.2	0.009	0.31	0.60 - 1.58	19.0	4.3
980805	17:31	4.1	0.019	0.33	1.49 - 1.88	25.9	9.1
200213	17:00	1.2	0.011	0.34	0.32 - 0.69	34.2	4.7
200303	18:15	1.2	0.018	0.34	0.50 - 0.96	25.9	10.4
200314	18:30	2.1	0.062	0.37	0.96 - 2.00	65.8	6.5
200315	17:00	2.0	0.012	0.33	0.40 - 0.72	24.6	7.1

The procedure begins by calculating spectral fluxes using MFRSR-measured surface albedos; calculations are made at the wavelengths observed by the RSS. Since the MFRSR albedos are measured at six discrete wavelengths (415, 500, 608, 664, 860, and 938 nm), they were linearly interpolated to the RSS wavelengths. Looping through each wavelength, modeled and observed spectral fluxes are compared and if the absolute value of the magnitude of the relative difference (in percent) is less than or equal to 0.1 (an arbitrary choice to quantify accuracy), the surface albedo at that wavelength remains unchanged. Otherwise, an improved initial estimate of albedo is determined by developing a simplistic linear relationship between downwelling flux and MFRSR albedo and the new estimate of surface albedo. If the model flux using the MFRSR albedo, F, is greater than the observed flux, R, then the

magnitude of the relative difference, at the very least, follows the relation F = R + 0.001 R; this value for F results in the desired accuracy between modeled and observed flux (conversely, if the model flux using the MFRSR albedo is less than the observed flux, then F = R - 0.001 R). This quantity can be equated to transmitted flux to the surface, T, divided by $(1-\alpha_s^*)$, where α_s^* is the improved initial estimate of albedo, i.e., $F = T/(1-\alpha_s^*)$. In a similar manner, $F_{mfrsr} = T/(1-\alpha_s)$ where α_s is the MFRSR albedo and F_{mfrsr}, the model flux using that albedo. Solving for T in both equations and equating the results leads to an improved initial estimate of surface albedo, namely, $\alpha_s^* = [F_{mfrsr}(1-\alpha_s) - F]/-F$. Using this method, a new set of surface albedos is generated and model fluxes using this initial "best-guess" set of reflectances is calculated. With model fluxes using MFRSR albedos and model fluxes using the improved estimates of surface albedos in place, the stage is set to proceed with Newton's scheme. Looping through each wavelength, the scheme is applied to each spectral group of fluxes and albedos in order to numerically determine a surface albedo such that the difference between the model flux and observed flux is less than 10^{-4} W/m^2. Convergence is generally achieved within five iterations. The final result is a set of surface albedos which, when used as input into an atmospheric model such as MODTRAN4, will yield downward fluxes at the surface matching the RSS observations.

Results

This method for estimating areal-mean surface albedo was validated using some field measurements taken on March 11-12, 2000. Using a spectrometer designed by Ocean Optics Inc., measurements of surface albedo over all basic surface types within the ARM Southern Great Plains (SGP) area were compiled. Landsat scenes available from the ARM external archive provided surface type classification. Albedo was retrieved by using the 6S radiative transfer code and atmospheric and aerosol data accessible from ARM SGP observations. The March 2000 measurements were used with the surface type classification from 1999 adjusted to early spring vegetation conditions to obtain areal-mean albedos as seen by a sensor at the cloud base altitude. Results are shown in Figure 2 for two springtime cases of March 3, 2000, and April 3, 1998, where the blue lines represent the spectral albedo derived from the method presented here and the green lines show the albedos independently derived from field measurements; MFRSR albedos are shown by the red lines. It is clear that the areal-mean albedos agree more closely together than do either, individually, to the MFRSR albedos. The spectral distribution of the areal-mean albedo is suggestive of a green vegetative surface whereas that from the MFRSR is representative of dry grass; this reflects the actual surfaces typically occurring during this season. Springtime growth is evident in the leftmost panel of Figure 1, which shows a Landsat image taken over the SGP area on April 4, 2000, so it is expected (and confirmed) that the areal-mean albedo would reflect this new green growth. Since the MFRSR instrument, installed on a 10-meter tower, overlooks an area of dry grass, the spectral distribution of the measured surface albedo reflects this. The new method of estimating areal-mean albedo reproduces surface reflectance quite well, representative of an area comparable to a model grid or a satellite pixel.

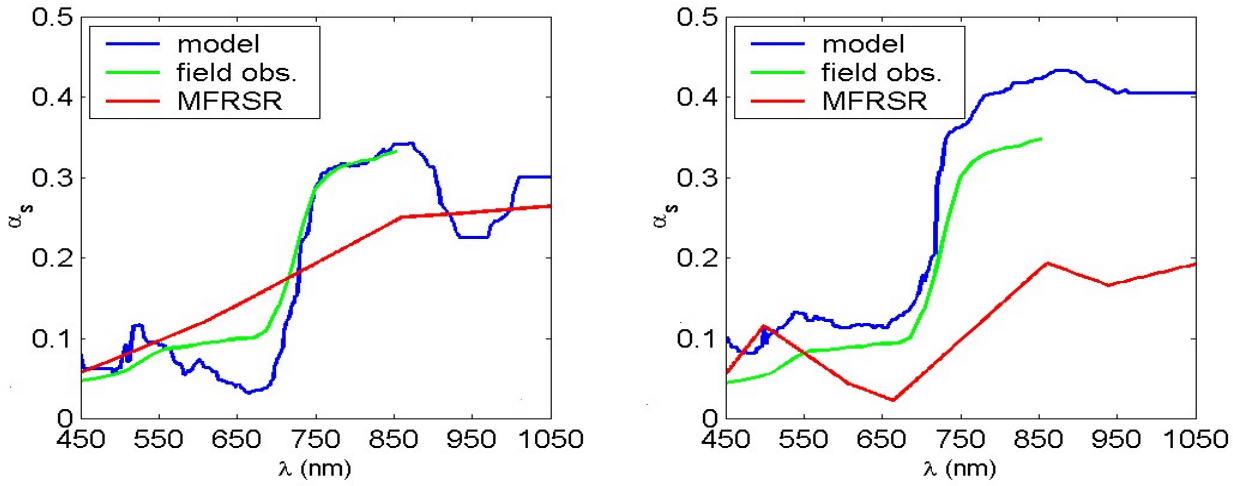

Figure 2. Validation of the proposed method for estimating areal-mean surface albedo, using measurements from a field campaign during March 2000. Method results (blue lines) are for the March 3, 2000, (left panel) and April 3, 1998, (right panel) cloud cases; MFRSR surface albedos for these cases are given by the red lines. The green lines show independently derived areal-mean albedos, generated from field measurements of surface albedo over typical surface types around the CF and surface type classification from Landsat data.

To gain a sense of the seasonal pattern of the areal-mean albedo, the method was applied to the cloudy cases in Table 1 and sample results for the different seasons are shown in Figure 3. Seasonal differences between areal-mean albedos and MFRSR point measurements of surface albedo over the CF are evident. Figure 4 focuses on the seasonal changes at two wavelengths; the multi-colored symbols denote the season: green circles (spring), blue triangles (summer), red asterisks (autumn), and black squares (winter). The left-hand panel shows a plot of areal-mean albedo as a function of MFRSR albedo in a visible wavelength; they agree reasonably well with absolute differences, generally less than 0.02. In the near-infrared (NIR) (right-hand panel), a more striking seasonal pattern arises with regard to differences between areal-mean albedos inferred from the RSS and point-wise albedos measured by the MFRSR. In the summer and fall, there is general agreement in NIR albedos. However, in the spring, the MFRSR underestimates NIR albedos with relative differences ranging from 30 - 120 percent; in winter, the underestimation is somewhat lessened, with relative differences between 24 and 70 percent. These trends can be explained by the land cover distribution in the area surrounding the CF and the physiological changes of the vegetation through the seasons. During the growth cycle of vegetation, reflectance increases in the NIR until the peak of its growth is reached; the estimation of springtime areal-mean albedo captures this behavior while the MFRSR instrument, trained over dry grass, simply cannot. Then with senescence during the fall and into the winter, there is a decrease in the NIR reflectance. Fields of winter wheat are present, so the landscape surrounding the CF is not completely deprived of green vegetation during the winter; hence the larger NIR albedos compared to those measured over dry grass by the MFRSR.

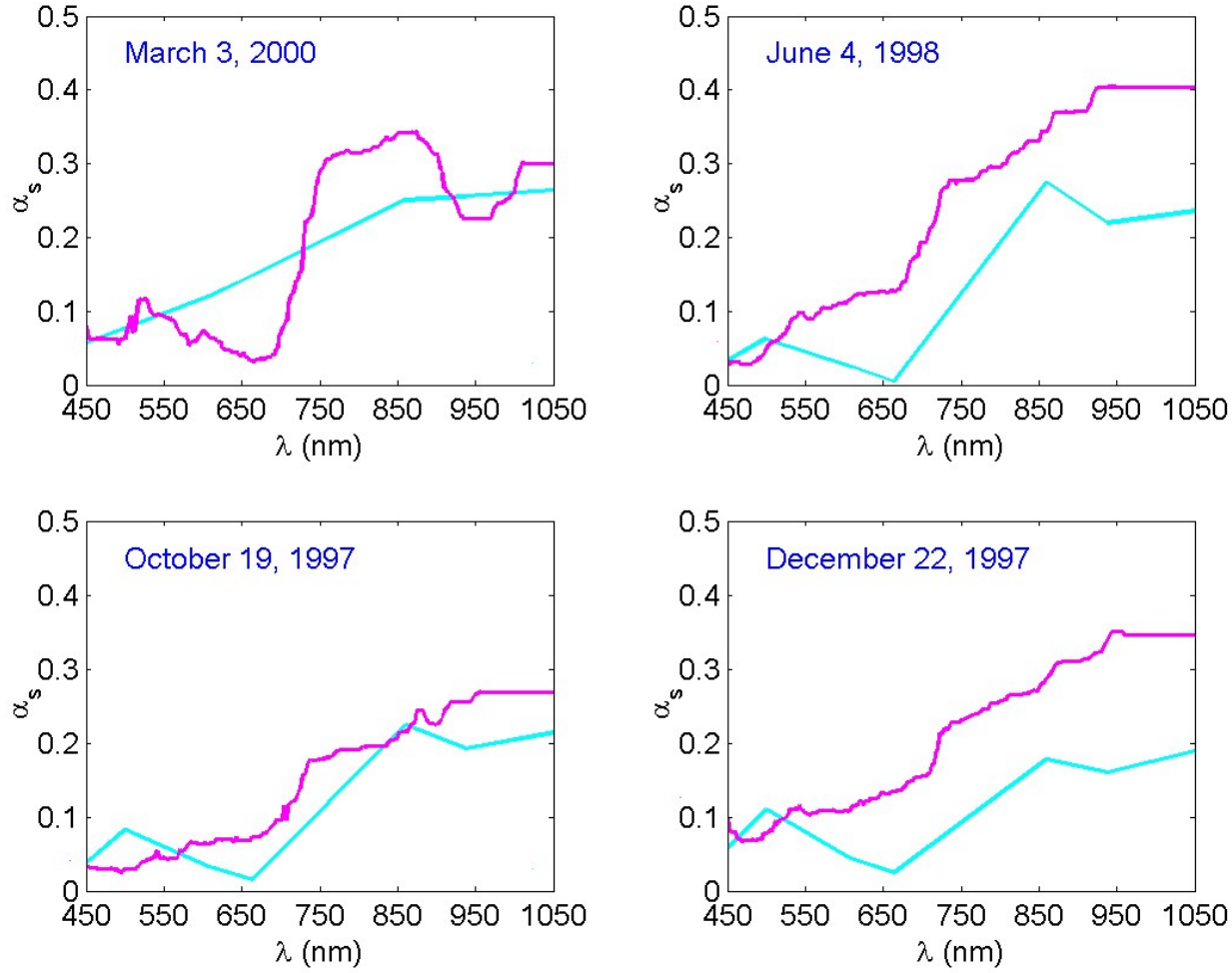

Figure 3. Surface albedo as a function of wavelength for cases in spring (upper left), summer (upper right), autumn (lower left) and winter (lower right). Shown are the MFRSR surface albedos (cyan lines) and the inferred areal-mean surface albedos (magenta lines).

Summary

A novel method to estimate areal-mean surface spectral albedo from downward surface irradiance measurements made under overcast conditions was presented. The method relies on good information on cloud parameters (LWP, r_e, etc.) extracted from such instruments as the MMCR and MWR and spectral transmittance of solar irradiance as measured by the RSS. The method is tested for overcast skies containing a low-level non-precipitating cloud. It was validated using some field campaign measurements and applied to numerous cloudy cases encompassing all seasons. The results were compared with point-wise surface albedo data deduced from upwelling and downwelling irradiance measured by the MFRSR.

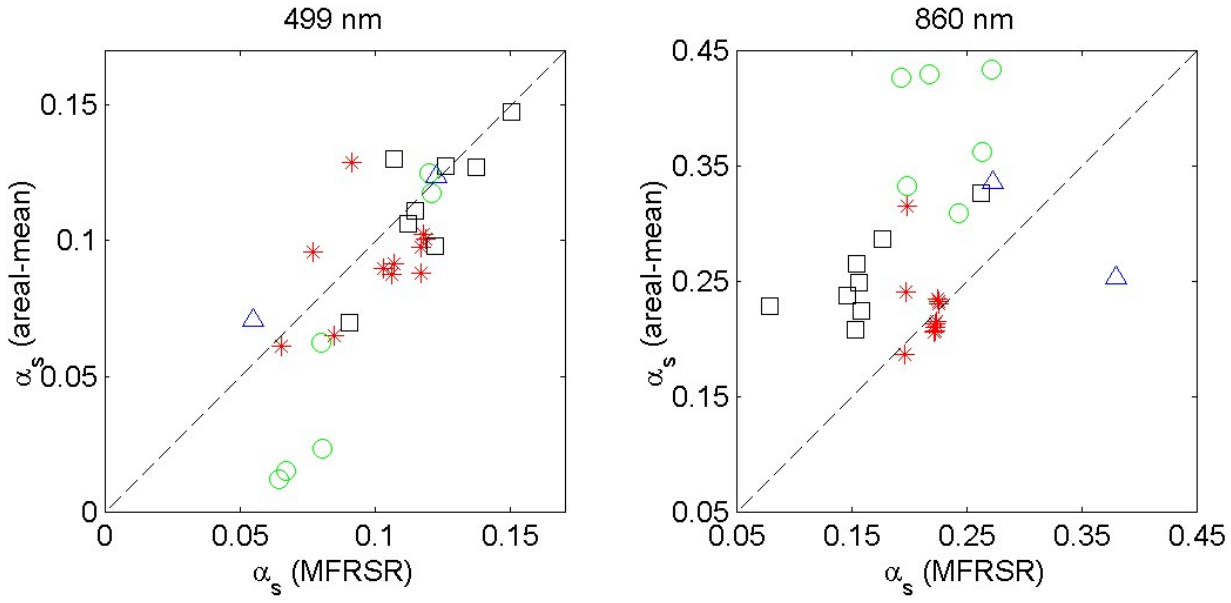

Figure 4. Adjusted surface albedo (areal-mean) as a function of MFRSR surface albedo in the visible and NIR spectra: green circles (spring), red asterisks (autumn), black squares (winter) and blue triangles (summer).

While visible albedo in the visible band agree reasonably well (absolute difference is less than 0.02), in the NIR, there is a more striking seasonal pattern with regard to differences between areal-mean albedos inferred from the RSS and point-wise albedos measured by the MFRSR. In spring, MFRSR measurements of NIR albedos are underestimated considerably with relative differences ranging from 30 percent to almost 120 percent, and to a lesser degree during winter months (with relative differences less than 70 percent). In summer and fall months, they generally agree well. The trend can be explained by the land cover distribution in the surrounding areas and the physiological changes of vegetation. The magnitudes of the discrepancies are so large that it should be taken into account in ARM modeling and remote sensing studies.

Acknowledgment

The study was supported by the U.S. Department of Energy under its ARM Program with Grant #DE-FG02-97ER62361.

Corresponding Author

Z. Li, zli@atmos.umd.edu, (301) 405-6699

References

Anderson, G. P., et al., 1999: MODTRAN4: Radiative transfer modeling for remote sensing. *Proc. SPIE, Optics in Atmospheric Propagation and Adaptive Systems III*, 3866, pp. 2-10.

Frisch, A. S., C. W. Fairall, and J. B. Snider, 1995: Measurement of stratus cloud and drizzle parameters in ASTEX with a K_α-band doppler radar and a microwave radiometer. *J. Atmos. Sci*., **52**, 2788-2799.

Harrison, L.C., J. J. Michalsky, Q. Min, and M. Beauharnois, 1998: Analysis of rotating shadowband spectroradiometer (RSS) data. In *Proceedings of the Eighth Atmospheric Radiation Measurement (ARM) Science Team Meeting*, DOE/ER-0738, pp. 773-776. U.S. Department of Energy, Washington, D.C. Available URL: http://www.arm.gov/docs/documents/technical/conf_9803/harrison-98.pdf

Ohmura, A., and H. Gilgren, 1993: Reevaluation of the global energy balance. *Interactions Between Global Climate Subsystems: The Legacy of Hann, Geophys. Monogr. Ser*., Vol. 75, eds. G. A. McBean and M.Hantel, AGU, pp. 93-110.